Chapter 1

Introduction

1.1 A Brief History of Neutrinos

The process of nuclear beta decay occurs when a neutron or proton inside an atomic nucleus changes into the other by either emitting or absorbing a beta particle (either an electron or positron). This process was initially conceptualized as a two-body decay, characterized by the emission of the beta particle with a discrete energy spectrum that is proportional to neutron-proton mass difference. However, it was observed that the emitted beta particles did not carry away enough energy and had a continuous energy spectrum. This prompted Wolfgang Pauli, the Austrian physicist, to postulate the presence of a new, extremely light, electrically neutral particle in 1930. The new particle, which was subsequently called the neutrino carries the missing energy and resolves the puzzle of non-conservation of energy in beta decay.

Enrico Fermi, in 1933, incorporated Pauli's hypothetical particle into his theory of beta decay. Fermi's beta decay theory accurately predicted the experimentally observed continuous energy spectrum associated with the decay of a neutron into a proton, electron, and anti-electron neutrino [1]. Due to their electrically neutral nature, neutrinos do not undergo electromagnetic interaction and remain unaffected by strong forces. In 1934, Bethe and Peierls discovered that the probability of a neutrino interacting with nuclei through the weak force is very low due to

their small interaction cross-sections [2]. Until 1956, the prevailing belief among physicists was that the detection of neutrinos in experiments was implausible. In 1946, Bruno Pontecorvo posited a prospective method for detecting neutrinos in large tanks of carbon tetrachloride containing chlorine atoms. When a neutrino interacts with a chlorine atom, it triggers an inverse beta decay, producing a radioactive argon atom. The subsequent decay of argon provides a detectable signal, indicating that the chlorine atom underwent an interaction with a neutrino.

$$\nu + {}^{37}\mathrm{Cl} \rightarrow e^- + {}^{37}\mathrm{Ar}. \tag{1.1}$$

In 1956, the evidence of neutrinos was first observed by Frederick Reines and Clyde Cowan [3]. In the nuclear reactor situated at the Savannah River site in South Carolina, they detected emitted antineutrinos via the following process

$$\bar{\nu} + p \rightarrow e^+ + n. \tag{1.2}$$

For this discovery, Frederick Reines later received the 1995 Nobel Prize in Physics.

Maurice Goldhaber, Lee Grodzins, and Andrew W. Sunyar made an important discovery that contributed significantly to the understanding of neutrino properties. In 1958 they studied the helicity of neutrinos and discovered that neutrinos were left-handed [4]. This experimental discovery and non-observation of right-handed neutrinos led to the understanding that neutrinos are massless.

After the discovery of neutrinos in 1956, Ray Davis built an experiment to measure neutrinos produced by the natural source: the Sun. Successful models at the time could explain how the neutrinos were produced by nuclear fusion in the core of the sun. The solar model was used to predict the amount of neutrinos that would be emitted by the sun. Davis built a large detector at the Homestake gold mine at Brookhaven National Laboratory to detect the solar neutrinos. However, he reported that only one-third of the predicted amount was observed [5]. This disagreement between the theory and experiment became known as the *Solar Neutrino Problem*. It was Pontecorvo who first pointed out that neutrinos could have multiple flavours which could explain the solar neutrino deficit. It was later discovered that neutrinos that interact with electrons and muons through charged

Group	No. of generators	No. of gauge bosons
$SU(3)_C$	8	8 gluons (massless)
$SU(2)_L$	3	W^+, W^-, and Z (massive)
$U(1)_Y$	1	γ (massless)

Table 1.1: Vector gauge bosons of the Standard Model of particle physics.

current are different, leading to the discovery of a different type of neutrino, ν_μ [6]. The experimental effort to make these discoveries was led by Leon Lederman, Melvin Schwartz, and Jack Steinberger at Brookhaven. Their contribution was awarded the Physics Nobel Prize in 1988.

The *Solar Neutrino Problem*, an issue that puzzled scientists for decades, was finally resolved through an improved understanding of neutrino properties at Sudbury Neutrino Oscillation (SNO) [7] and Super-Kamiokande (SK) [8] collaborations. It was observed that in SNO using heavy water as detector, certain interactions were caused by only electron neutrinos, while other interactions were caused by all neutrino flavors. By comparing the total number of solar neutrinos (all flavors) to the number of solar electron neutrinos, scientists were able to calculate the total number of neutrino interactions, which now matched the predictions from the solar neutrino model. The number of ν_e interactions also matched the number predicted by the experiment conducted by Davis. The anticipation of a shortage in electron neutrinos arose from the formulation of the Mikheyev-Smirnov-Wolfenstein (MSW) effect in 1985 [9, 10]. MSW effect suggests that as the neutrinos propagate through matter, the neutrinos undergo oscillation and change from one flavour to another.

In 2000, the Direct Observation of NU Tau (DONUT) collaboration identified the tau neutrino as the third type of neutrino [11]. The detection was accomplished by observing the decay of charmed particles, generating tau neutrinos and affirming the existence of three distinct neutrino flavors. The SK and SNO collaborations conducted pioneering oscillation experiments, providing robust statistical

evidence for neutrino oscillations. Subsequently, numerous additional neutrino experiments have contributed significantly to expanding our comprehension of neutrino properties.

1.2 Neutrinos in the Standard Model

There exist four fundamental forces, identified as strong, electromagnetic, weak, and gravity within the realm of our current understanding. The Standard Model explains how elementary particles interact through strong, electromagnetic, and weak forces. It is formulated as a gauge theory based on the group $SU(3)_C \times SU(2)_L \times U(1)_Y$, where the subscripts C, L, and Y correspond to color charge, left-handed chirality, and weak hypercharge respectively. Particles are divided into two groups: fermions and bosons. Fermions, which constitute matter, are divided into quarks and leptons. Quarks, such as up (u), down (d), charm (c), strange (s), top (t), and bottom (b), have fractional electric charges and participate in strong interactions mediated by gluons. Leptons, including the electron (e), muon (μ), tau (τ) have integer electric charges, and their corresponding neutrinos ($\nu_e,\ \nu_\mu,\ \nu_\tau$), which are neutral particles, interact via weak and electromagnetic forces. The SM incorporates four types of gauge bosons that act as force carriers: the photon (γ), which mediates electromagnetic interactions between charged particles, and the W^+, W^-, and Z^0 bosons, which mediate the weak interactions. In addition, eight massless gluons govern the strong force, binding quarks within protons, neutrons, and other hadrons. The gauge group determines the interactions and the quantity of vector gauge bosons. We have summarized this in Table 1.1.

The SM also introduces the Higgs mechanism, which explains how gauge bosons acquire mass through spontaneous symmetry breaking. This mechanism postulates the existence of the Higgs field, spread throughout the universe, and its corresponding particle, the Higgs boson. Interaction of particles with this field imparts mass to some particles, while others, like photons, remain massless. The

Field	Generations	$SU(3)_C \times SU(2)_L \times U(1)_Y$
l_L	3	(1, 2, -$\frac{1}{2}$)
E_R	3	(1, 1, -1)
Q_L	3	(3, 2, $\frac{1}{6}$)
U_R	3	(3, 1, $\frac{2}{3}$)
D_R	3	(3, 1, -$\frac{1}{3}$)
Φ	1	(1, 2, $\frac{1}{2}$)

Table 1.2: Fields of the SM and their transformation properties.

predictions put forth by the Standard Model have been validated by a multitude of experimental observations. The construction of the Large Hadron Collider (LHC) at CERN was designed to ascertain the last elusive facet of this theoretical framework. The findings derived from the LHC experiments unequivocally confirmed the presence of the Higgs boson. The particle content and their transformation properties under the SM gauge group are given in Table 1.2, where $L(R)$ indicates the left (right) chiral projections and Φ is the Higgs field.

Despite its success in describing the masses of SM-charged fermions and gauge bosons, the Standard Model predicts that neutrinos are massless. However, there are many shortcomings to the SM, and it is far from providing a complete picture. In contrast to the prediction from SM, evidence from various neutrino oscillation experiments suggests that neutrinos have non-zero masses and their flavours mix [12–15]. This is an experimental proof of physics Beyond the Standard Model (BSM).

1.2.1 The Electroweak Theory

The electroweak theory is a key component of the Standard Model (SM) of particle physics. It unifies two of the fundamental forces, electromagnetism, and the weak nuclear force. The theory arises from the symmetry group $SU(2)_L \times U(1)_Y$, where

$SU(2)_L$ represents weak isospin and $U(1)_Y$ corresponds to weak hypercharge. The Electroweak Theory explains particle interactions through the exchange of force-carrying bosons: the $W^{\pm}$ and Z bosons for weak interactions, and the photon (γ) for electromagnetic interactions. The electroweak interaction is governed by a gauge-invariant, renormalizable Lagrangian

$$\mathcal{L} = \mathcal{L}_F + \mathcal{L}_G + \mathcal{L}_\Phi + \mathcal{L}_Y. \tag{1.3}$$

The terms that present the kinetic interactions of fermion fields are

$$\mathcal{L}_F = \bar{Q}_L i\not{D} Q_L + \bar{l}_L i\not{D} l_L + \bar{U}_R i\not{\partial}' U_R + \bar{D}_R i\not{\partial}' D_R + \bar{E}_R i\not{\partial}' E_R, \tag{1.4}$$

where

$$\begin{aligned} \not{D} &\equiv D_\mu \gamma^\mu = \left(\partial_\mu - ig\tau^k W_\mu^k - ig' Y B_\mu\right)\gamma^\mu, \\ \not{\partial}' &\equiv \partial'_\mu \gamma^\mu = \left(\partial_\mu - ig' Y B_\mu\right)\gamma^\mu \end{aligned} \tag{1.5}$$

with $\tau_k = \sigma_k/2$ ($k = 1, 2, 3$) and Y are the generators of the groups $SU(2)_L$ and $U(1)_Y$, respectively. g and g' are the coupling constants. The kinetic interactions the gauge fields are governed by

$$\mathcal{L}_G = -\frac{1}{4} W^{i\mu\nu} W^i_{\mu\nu} - \frac{1}{4} B^{\mu\nu} B_{\mu\nu}. \tag{1.6}$$

where

$$\begin{aligned} W^i_{\mu\nu} &= \partial_\mu W^i_\nu - \partial_\nu W^i_\mu + g\varepsilon^{ijk} W^j_\mu W^k_\nu, \\ B_{\mu\nu} &= \partial_\mu B_\nu - \partial_\nu B_\mu, \end{aligned} \tag{1.7}$$

with W^i_μ ($i = 1, 2, 3$) and B_μ are the $SU(2)_L$ and $U(1)_Y$ gauge bosons, respectively. The interactions of the scalar fields are given by

$$\mathcal{L}_\Phi = \left(D^\mu \Phi\right)^\dagger \left(D_\mu \Phi\right) - \mu^2 \Phi^\dagger \Phi - \lambda \left(\Phi^\dagger \Phi\right)^2 \tag{1.8}$$

where μ^2 and $\lambda > 0$ is real. The Yukawa interactions that generate the quark and charged lepton masses are

$$\mathcal{L}_Y = -\bar{Q}_L Y_u \tilde{\Phi} U_R - \bar{Q}_L Y_d \Phi D_R - \bar{l}_L Y_l \Phi E_R + h.c., \tag{1.9}$$

where $\tilde{\Phi} = i\sigma_2\Phi^*$, Φ^* is the charge conjugate of the Higgs field and Y_u, Y_d, Y_l are the Yukawa coupling matrices.

It has been observed that weak interactions can only occur through the mediation of massive gauge bosons. The mass of the vector bosons is generated through spontaneous symmetry breaking (SSB) and is introduced in the Higgs sector. One way to achieve symmetry breaking is by introducing a doublet scalar, $\Phi = (\phi^+, \phi^0)^T$. The last two terms of equation (1.8) describe the renormalizable, gauge-invariant Higgs potential. To determine the VEV, we need to minimize the Higgs potential. For $\mu^2 > 0$, no SSB occurs, and $\langle\Phi\rangle_0 = 0$. However, for $\mu^2 < 0$, EWSB occurs, and we obtain the vacuum of the theory $\langle\Phi\rangle_0 = (0,\ v/\sqrt{2})^T$, with $v = \sqrt{-\mu^2/\lambda}$. The VEV breaks $SU(2)_L \times U(1)_Y$ into $U(1)_Q$. After spontaneous symmetry breaking, $\Phi \to \Phi' = \frac{1}{\sqrt{2}}(0,\ v + h)^T$, the following consequences are observed.

1. From the first term in equation (1.8), we get the masses of the gauge bosons

$$(D^\mu\Phi)^\dagger (D_\mu\Phi) = M_W^2 W^{\mu+} W_\mu^- + \frac{1}{2} M_Z^2 Z_\mu Z^\mu \tag{1.10}$$

   where $W^\pm = \frac{1}{\sqrt{2}}(W^1 \mp iW^2)$ and $Z = -\sin\theta_W B + \cos\theta_W W^3$ are the W and Z gauge bosons, respectively; θ_W is the Weinberg angle and is defined as $\tan\theta_W = \frac{g'}{g}$. The mass of the W and Z gauge bosons are $M_W = \frac{gv}{2}$ and $M_Z = \sqrt{g^2 + g'^2}\frac{v}{2}$. The photon field $A = \cos\theta_W B + \sin\theta_W W^3$ remains massless.

2. Equations (1.4) and (1.6), which represent the kinetic terms of the fermionic and gauge fields, are converted into the weak neutral current (NC) interactions involving Z bosons, the weak charge current (CC) interactions involving W bosons, and the quantum electrodynamics (QED) interactions involving photons. We acquire the subsequent Lagrangian

$$\mathcal{L}_{QED} = -\frac{gg'}{\sqrt{g^2 + g'^2}} J_Q^\mu A_\mu, \tag{1.11}$$

   where

$$J_Q^\mu = \frac{2}{3}(\bar{u}\ \bar{c}\ \bar{t})\,\gamma^\mu \begin{pmatrix} u \\ c \\ t \end{pmatrix} - \frac{1}{3}(\bar{d}\ \bar{s}\ \bar{b})\,\gamma^\mu \begin{pmatrix} d \\ s \\ b \end{pmatrix} - (\bar{e}\ \bar{\mu}\ \bar{\tau})\,\gamma^\mu \begin{pmatrix} e \\ \mu \\ \tau \end{pmatrix} \tag{1.12}$$

The weak CC and NC interactions are given by

$$\mathcal{L}_{CC} = -\frac{g}{2\sqrt{2}} J_W^\mu W_\mu^+ + h.c., \tag{1.13}$$

and

$$\mathcal{L}_{NC} = -\frac{g}{4\cos\theta_W} J_Z^\mu Z_\mu + h.c., \tag{1.14}$$

where

$$J_W^\mu = (\bar{\nu_e}\ \bar{\nu_\mu}\ \bar{\nu_\tau})\,\gamma^\mu(1-\gamma^5)\begin{pmatrix} e \\ \mu \\ \tau \end{pmatrix} + (\bar{u}\ \bar{c}\ \bar{t})\,\gamma^\mu(1-\gamma^5)\begin{pmatrix} d \\ s \\ b \end{pmatrix}, \tag{1.15}$$

$$\begin{aligned} J_Z^\mu = {} & (\bar{u}\ \bar{c}\ \bar{t})\,\gamma^\mu(1-\gamma^5)\begin{pmatrix} u \\ c \\ t \end{pmatrix} - (\bar{d}\ \bar{s}\ \bar{b})\,\gamma^\mu(1-\gamma^5)\begin{pmatrix} d \\ s \\ b \end{pmatrix} \\ & + (\bar{\nu_e}\ \bar{\nu_\mu}\ \bar{\nu_\tau})\,\gamma^\mu(1-\gamma^5)\begin{pmatrix} \nu_e \\ \nu_\mu \\ \nu_\tau \end{pmatrix} - (\bar{e}\ \bar{\mu}\ \bar{\tau})\,\gamma^\mu(1-\gamma^5)\begin{pmatrix} e \\ \mu \\ \tau \end{pmatrix} - 4\sin^2\theta_W J_Q^\mu. \end{aligned} \tag{1.16}$$

3. From equation (1.9), we get the masses of the six quarks and the charged leptons. The Yukawa Lagrangian becomes

$$\mathcal{L}_Y = -\bar{U}_R M_u U_L - \bar{D}_R M_d D_L - \bar{E}_R M_l E_L + h.c., \tag{1.17}$$

where the up-type quarks, down-type quarks, and charged leptons mass matrices are

$$M_u = \frac{1}{\sqrt{2}} v Y_u, \qquad M_d = \frac{1}{\sqrt{2}} v Y_d, \qquad M_l = \frac{1}{\sqrt{2}} v Y_l, \tag{1.18}$$

As can be seen from the above consequences of the Higgs mechanism, neutrinos have no mass in the standard model because there are no right-handed (RH) neutrinos in the Standard Model.

1.3 Neutrinos Beyond the Standard Model

1.3.1 Neutrino Oscillations

Neutrinos come in three different flavours: electron neutrinos (ν_e), muon neutrinos (ν_ν), and tau neutrinos (ν_τ). As the neutrinos travel through space they change from one flavour to another, this flavour changing process is known as neutrino

oscillations. Neutrino oscillations were first theorized by Bruno Pontecorvo in 1957 and experimentally confirmed in 1998, marking a fundamental discovery in particle physics. The reason for this is that neutrinos have a small mass, and their flavor and mass eigenstates are not the same. The flavor eigenstates of the three neutrinos are denoted as $(\nu_e,\ \nu_\mu,\ \nu_\tau)$, and the mass eigenstates are denoted as $(\nu_1,\ \nu_2,\ \nu_3)$, with corresponding eigenvalues of $(m_1,\ m_2,\ m_3)$. The Pontecorvo-Maki-Nakagawa-Sakata (PMNS) matrix is a 3×3 unitary matrix that determines the mismatch between the flavour and mass eigenstates of neutrinos. [16].

$$\begin{pmatrix} \nu_e \\ \nu_\mu \\ \nu_\tau \end{pmatrix} = U_{\text{PMNS}} \begin{pmatrix} \nu_1 \\ \nu_2 \\ \nu_3 \end{pmatrix}$$

$$\begin{pmatrix} \nu_e \\ \nu_\mu \\ \nu_\tau \end{pmatrix} = \begin{pmatrix} U_{e1} & U_{e2} & U_{e3} \\ U_{\mu 1} & U_{\mu 2} & U_{\mu 3} \\ U_{\tau 1} & U_{\tau 2} & U_{\tau 3} \end{pmatrix} \begin{pmatrix} \nu_1 \\ \nu_2 \\ \nu_3 \end{pmatrix} \tag{1.19}$$

The U_{PMNS} can be parametrized by three rotation matrices and is known as the standard parametrization prescribed by the Particle Data Group [17]

$$U_{\text{PMNS}} = \begin{pmatrix} 1 & 0 & 0 \\ 0 & c_{23} & s_{23} \\ 0 & -s_{23} & c_{23} \end{pmatrix} \begin{pmatrix} c_{13} & 0 & s_{13}e^{-i\delta} \\ 0 & 1 & 0 \\ -s_{13}e^{i\delta} & 0 & c_{13} \end{pmatrix} \begin{pmatrix} c_{12} & s_{12} & 0 \\ -s_{12} & c_{12} & 0 \\ 0 & 0 & 1 \end{pmatrix} P_M \tag{1.20}$$

where $c_{ij} = \cos\theta_{ij},\ s_{ij} = \sin\theta_{ij}$ (for $ij = 12, 13, 23$), δ is the Dirac CP phase and $P = \text{diag}(1,\ e^{i\alpha_{21}/2},\ e^{i\alpha_{31}/2})$ with α_{21}, α_{31} are the Majorana phases. The presence of the Majorana phases characterizes Majorana nature of neutrinos.

1.3.2 Neutrino Oscillation Probability

The neutrino of a particular flavour α and momentum $\vec{p}$, created in a charged-current weak interaction propagate as the mass states $|\nu_k\rangle$. The mass state evolve as follows

$$\frac{\partial}{\partial t}|\nu_k\rangle = iH|\nu_k\rangle, \tag{1.21}$$

where $k = 1, 2, 3$ and the solutions suggest that the mass states evolve in time as plane waves of the form

$$|\nu_k(t)\rangle = e^{-iE_k t}|\nu_k\rangle. \tag{1.22}$$

Let us denote a neutrino created with a definite flavour α by $|\nu_\alpha(t)\rangle$, then the time evolution of this state is written as

$$|\nu_\alpha(t)\rangle = \sum_k U^*_{\alpha k} e^{-iE_k t}|\nu_k\rangle \tag{1.23}$$

such that

$$|\nu_\alpha(t=0)\rangle = |\nu_\alpha\rangle \tag{1.24}$$

Since U is unitary in nature, the mass states may be written as

$$|\nu_k\rangle = \sum_\alpha U_{\alpha k}|\nu_\alpha\rangle \tag{1.25}$$

Now, substituting equation (1.25) into equation (1.23), we get

$$|\nu_\alpha(t)\rangle = \sum_{\beta=e,\mu,\tau}\left(\sum_k U^*_{\alpha k} e^{-iE_k t} U_{\beta k}\right)|\nu_k\rangle. \tag{1.26}$$

We wish to calculate the probability that, while travelling a distance L, a neutrino with flavour α would oscillate and transform into a neutrino with flavour β. The amplitude of the transition $\nu_\alpha \to \nu_\beta$ is given by

$$\langle\nu_\beta|\nu_\alpha(t)\rangle = \sum_k U^*_{\alpha k} U_{\beta k} e^{-iE_k t}. \tag{1.27}$$

For ultrarelativistic neutrinos, we can use the approximation

$$E_k \simeq E + \frac{m_k^2}{2E}. \tag{1.28}$$

thus,

$$E_k - E_k \simeq \frac{\Delta m^2_{kj}}{2E}, \tag{1.29}$$

where $\Delta m^2_{kj} = m^2_k - m^2_j$ is the mass-squared difference and $E = |\vec{p}|$. Therefore, the transition probability may be approximated as

$$P_{\nu_\alpha\to\nu_\beta}(t) = |\langle\nu_\beta|\nu_\alpha(t)\rangle|^2 = \sum_{k,j} U^*_{\alpha k} U_{\beta k} U_{\alpha j} U^*_{\beta j} \exp\left(-i\frac{\Delta m^2_{kj} t}{2E}\right) \tag{1.30}$$

In the approximation of ultrarelativistic neutrinos, they travel with the speed of light thus, it is justified to take $t = L$

$$P_{\nu_\alpha \to \nu_\beta}(t) = \sum_{k,j} U^*_{\alpha k} U_{\beta k} U_{\alpha j} U^*_{\beta j} \exp\left(-i \frac{\Delta m^2_{kj} L}{2E}\right) \tag{1.31}$$

With further simplification, the oscillation probability becomes

$$\begin{aligned} P_{\nu_\alpha \to \nu_\beta} = \delta_{\alpha\beta} &- 4 \sum_{k>j} \mathrm{Re}\left[U^*_{\alpha k} U_{\beta k} U_{\alpha j} U^*_{\beta j}\right] \sin^2\left(\frac{\Delta m^2_{jk} L}{4E}\right) \\ &+ 2 \sum_{k>j} \mathrm{Im}\left[U^*_{\alpha k} U_{\beta k} U_{\alpha j} U^*_{\beta j}\right] \sin\left(\frac{\Delta m^2_{jk} L}{2E}\right) \end{aligned} \tag{1.32}$$

The probability of oscillation depends on various factors, including the mixing angles, the difference in mass squared between the neutrinos, the energy of the neutrinos, and the distance between where the neutrinos are produced and where they are detected. By determining the probability of oscillation for different types of neutrino flavour transitions, the oscillation parameters can be measured. In typical experiments, the distance from production to detection remains constant, while the energy of neutrinos is altered. Furthermore, the detection of neutrino oscillations implies the existence of at least two non-zero mass eigenstates.

1.4 Review of Neutrino Parameters

In the field of experimental neutrino physics, one of the most significant achievements has been the validation of Pontecorvo's prediction regarding neutrino oscillation. This discovery has not only confirmed theoretical ideas but has also opened doors for deeper investigation into the complex characteristics of neutrinos. In the last five decades, various experimental efforts have been made to accurately measure the parameters of neutrinos. In this section, we aim to provide a concise summary of the historical advancements in oscillation experiments employed for exploring atmospheric, reactor, and solar neutrino parameters. Additionally, we will discuss their present status.

1.4.1 Solar Neutrino Experiments

The reactions that occur in the core of the sun produce electron neutrinos. The dominant reactions that produce the solar neutrinos are given as follows

$$\begin{aligned} p + p &\rightarrow {}^{2}\mathrm{H} + e^{+} + \nu_e, \\ p + e^{-} + p &\rightarrow {}^{2}\mathrm{H} + \nu_e, \\ {}^{7}\mathrm{Be} + e^{-} &\rightarrow {}^{7}\mathrm{Li} + \nu_e, \\ {}^{8}\mathrm{B} &\rightarrow {}^{8}\mathrm{Be}^{*} + e^{+} + \nu_e \end{aligned}$$

Solar neutrinos were first discovered in the Homestake experiment in 1970 [18]. It was observed that the solar neutrinos were in deficit and this fact was later observed in many other experiments such as GALLEX [19], GNO [20], and SAGE [21]. The detection of the solar neutrinos in these experiments involves the following reaction

$$^{71}\mathrm{Ga} + \nu_e \rightarrow {}^{71}\mathrm{Ge} + e^{-}$$

The Kamiokande and Super-Kamiokande (SK) collaborations also detected the solar neutrino anomaly. The solar electron neutrinos produced in the sun are converted into other types of neutrinos as they travel through space and reach the detectors placed on Earth. Experiments such as SNO and SK provided substantial evidence of $\nu_e \rightarrow \nu_\mu$ and $\nu_e \rightarrow \nu_\tau$ transitions.

The KamLAND experiment, located in Japan, detects MeV-scale reactor neutrinos at a 180km baseline, providing precise measurements of solar neutrino parameters. The best-fit values of the solar neutrino parameters from the global fit of solar experimental data are $\Delta m_{sol} \simeq 7.49 \times 10^{-5}$ eV^2 and $\theta_{12} \simeq 33.72^{\circ}$.

When high-energy cosmic rays from space collide with the Earth's atmosphere, a series of particle events occur. These events lead to the creation of atmospheric neutrinos, muons, and muon neutrinos. Two basic mechanisms contribute to the creation of atmospheric neutrinos-pion and kaon decay. Protons make up the majority of cosmic rays, and Figure 1.1 illustrates how these protons are converted into atmospheric neutrinos.

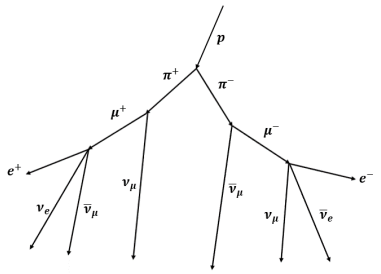

Figure 1.1: Diagram representing the production of atmospheric neutrinos from the cosmic ray protons.

1.4.2 Atmospheric Neutrino Experiments

The neutrinos generated in these reactions have energies of about 100 MeV to about 100 GeV. In 1965 the Kolar Gold Field Mine in India [22, 23] and the East Rand Proprietary Gold Mine in South Africa first reported the citing of atmospheric neutrinos. Numerous experiments, such as NUSSEX, Frejus, Soudan [24], and SK, were constructed to detect atmospheric neutrinos. In 1988, the Kamiokande team found that, based on the current understanding of atmospheric fluxes, the anticipated proportion of muon to electron neutrino was $\approx 60\%$ of the anticipated event count.[25]. The current detectors can differentiate between the upward-going and the downward-going muons (secondary cosmic-ray muons). Both an up-down asymmetry and a deficit in the muon neutrino flow were found by SK in 1998. This finding supported the idea that whereas down-going neutrinos do not have enough distance to oscillate into a new flavour, up-going muon neutrinos oscillate into tau neutrinos. Analysis of the data revealed atmospheric parameters, with Δm^2_{atm} approximately equal to 2.4×10^{-3} eV^2 and θ_{23} around $\pi/4$.

There are several accelerator-based experiments like Tokai to Kamioka (T2K) [26], Main Injector Neutrino Oscillation Search (MINOS) [27], and NuMI Off-Axis ν_e Appearance (NOνA) [28] measuring the atmospheric neutrino parameters.

The T2K experiment utilizes a powerful neutrino beam that is generated at

the Japan Proton Accelerator Research Complex (J-PARC) in Tokai, Japan. This beam is created by colliding protons from the J-PARC accelerator with a target, which produces mesons that decay into neutrinos. After being created, the neutrino beam is directed towards a specific location. To better understand the beam, its properties are measured at J-PARC using the Interactive Neutrino GRID (INGRID) near detector system before it reaches the far detector. The neutrino beam travels over a distance of approximately 295 kilometers through the Earth to reach the Super-Kamiokande detector, which is located in the Kamioka mine. The Super-Kamiokande detector can detect Cherenkov radiation from charged particles generated in neutrino interactions. T2K is designed to monitor the oscillation of muon neutrinos into electron neutrinos. By comparing the predicted and actual rates of neutrino interactions at the distant detector, scientists can deduce the characteristics of neutrino oscillation, such as mixing angles and mass differences.

The MINOS experiment aimed to investigate the transformation of muon neutrinos into other types of neutrinos. It was conducted at the Fermi National Accelerator Laboratory (Fermilab) in the United States. To create an intense muon neutrino beam, the experiment used the NuMI (Neutrinos at the Main Injector) beamline at Fermilab. Protons from the Fermilab Main Injector accelerator were directed onto a target, producing mesons that decayed to form a muon neutrino beam. The Near Detector, located at Fermilab near the production point, measured the properties of the original beam of neutrino before its oscillation. After travelling nearly 735 km through the Earth, the muon neutrino beam reached the distant detector at the Soudan Underground Laboratory in Minnesota. The Far Detector, located deep below the surface, was built to detect charged particles resulting from neutrino interactions. The goal of the MINOS experiment was to track the oscillation of muon neutrinos as they travelled from the near detector to the distant detector, changing into other neutrino types like electron or tau neutrinos. Scientists compared the neutrino flux and spectrum at the near and distant detectors to identify the characteristics of oscillation, such as mass differences and mixing angles. NOνA generates a high-intensity muon neutrino beam at

Fermilab using the NuMI beamline. Mesons are produced when protons from the Fermilab Main Injector accelerator are directed toward a target. As these mesons decay, a muon neutrino beam is created. Two massive detectors are used in the NOνA experiment: the Near Detector, which is located near Fermilab's neutrino production site, and the Far Detector, which is located in Ash River, Minnesota, approximately 810 kilometers distant. The neutrino beam's initial characteristics are described by the Near Detector before oscillations happen. The goal of NOνA is to track the oscillation of electron neutrinos from muon neutrinos. Scientists may determine neutrino oscillation parameters like mixing angles and mass differences by comparing the neutrino beam's characteristics at the Near Detector with those seen at the Far Detector.

The latest research indicates that the data obtained from MINOS and T2K aligns with the maximal atmospheric mixing angle. However, NOνA contradicts maximal mixing at a significance level of 2.6 σ.

1.4.3 Reactor Neutrino Experiments

As a result of nuclear fission, nuclear reactors generate a significant amount of antineutrinos. The beta decay of fission products is the main source of neutrinos produced in reactors. Therefore, reactor neutrino experiments play an important role in the precision measurement of θ_{13}. Each fission process generates six electron antineutrinos and about 200 MeV thermal power. The antineutrino flux is isotropic and this means that it decreases rapidly with distance. This makes studying neutrino oscillation very difficult as oscillation requires an appropriate distance between the source and the detector. Now, the energy of the reactor antineutrino is of the order of a few MeV, therefore their oscillation length is relatively short and only $\bar{\nu}_e$ disappearance can be examined in the reactor experiment. Reactor neutrino experiments aim to capture the antineutrinos released by nuclear reactors by placing a near detector. The most prevalent interaction for reactor antineutrinos is the inverse beta decay mechanism. A positron and a neutron are

created during this process when an antineutrino interacts with a proton.

$$\bar{\nu}_e + p \rightarrow n + e^+$$

Two gamma rays are produced when the positron from the IBD process annihilates with an electron. More gamma rays are released when the neutron is taken up by adjacent nuclei. The energies of the neutrino and positron are [1]

$$E_\nu = E_e + T_n + m_n - m_p \simeq E_e + 1.293\text{MeV}, \tag{1.33}$$

where T_n recoil kinetic energy of the neutron, is very small. Therefore, we can write the threshold neutrino energy as

$$E_\nu^{th} = \frac{(m_n + m_e)^2 - m_p^2}{2m_p} \simeq 1.806\text{MeV} \tag{1.34}$$

This implies that only $\sim 25\%$ of the antineutrino produced in the reactor can be detected.

For a long time, it was believed that the reactor mixing angle $\theta_{13} = 0$. This made the measurement and understanding of the reactor mixing angle θ_{13} that much more significant. One of the first experiments to investigate neutrino oscillations was the Chooz experiment, which is located at the Chooz Nuclear Power Station in France [29]. Its precise goal was to calculate the mixing angle θ_{13}. Due to insufficient statistics, the experiment established a maximum value for θ_{13} but failed to yield a meaningful measurement. The Double Chooz experiment, situated at the Chooz Nuclear Power Station, commenced data collection in 2011 with enhanced statistics and sensitivity. The first non-zero measurement of θ_{13} was released by the Double Chooz team in 2012, offering crucial evidence for neutrino oscillations using electron antineutrinos [30]. Another experiment started data gathering in 2011, the Daya Bay experiment—situated at the Daya Bay Nuclear Power Plant in China—quickly rose to prominence in the field. Daya Bay published an accurate measurement of the mixing angle θ_{13} in 2012 [31]. Their results were comparable with prior observations from Double Chooz and offered a more

[1] The recoil energy of the neutron is small and neglected in this calculation.

precise estimation of the parameter. Data collection for the RENO experiment, situated at the Hanbit Nuclear Power Complex in South Korea, also commenced in 2011. The mixing angle θ_{13}, with a different baseline than the previous experiments, was announced by RENO in 2012 [32]. The outcome agreed with Daya Bay and Double Chooz's measures. Global analyses including data from several experiments, such as reactor and accelerator-based studies, have been conducted, and the measurements of θ_{13} and other neutrino oscillation parameters are improved, leading to a more thorough knowledge of neutrino physics.

1.4.4 CP Violation in the Leptonic Sector

With the discovery of non-zero θ_{13} and precision measurement $\theta_{13} \simeq 8.5°$, it paved the way to explore the leptonic CP violation through the measurement of δ_{CP}. The measurement of δ_{CP} is not as well established as other neutrino oscillation parameters. The current results on δ_{CP} suggest that at 3σ level it allows for both maximal CP-violation and CP-conservation. However, recent results from T2K suggest that there is a slight preference towards maximal CP violation.

At the Sanford Underground Research Facility (SURF) in South Dakota, USA, a massive neutrino experiment known as the Deep Underground Neutrino Experiment (DUNE) is currently being built. Measurement of neutrino characteristics, detection of proton decay, and the search for leptonic CP violation are among the unresolved topics in neutrino physics that DUNE seeks to resolve. Sanford Underground Research Facility (SURF) in South Dakota will host detectors for the experiment, which will make use of a long-baseline configuration with a neutrino beam coming from Fermilab in Illinois. To maximize sensitivity to δ_{CP}, several neutrino beam configurations will be investigated, including changes in the beam's energy and intensity. DUNE features four huge liquid argon time-projection chambers (LArTPCs) as detectors. Two of these detectors will be located at SURF as the Far Detector complex, while the other two will function as the Near Detector complex at Fermilab. To precisely ascertain if δ_{CP} takes values that deviate from CP symmetry, the experiment strives for a high degree of sensitivity.

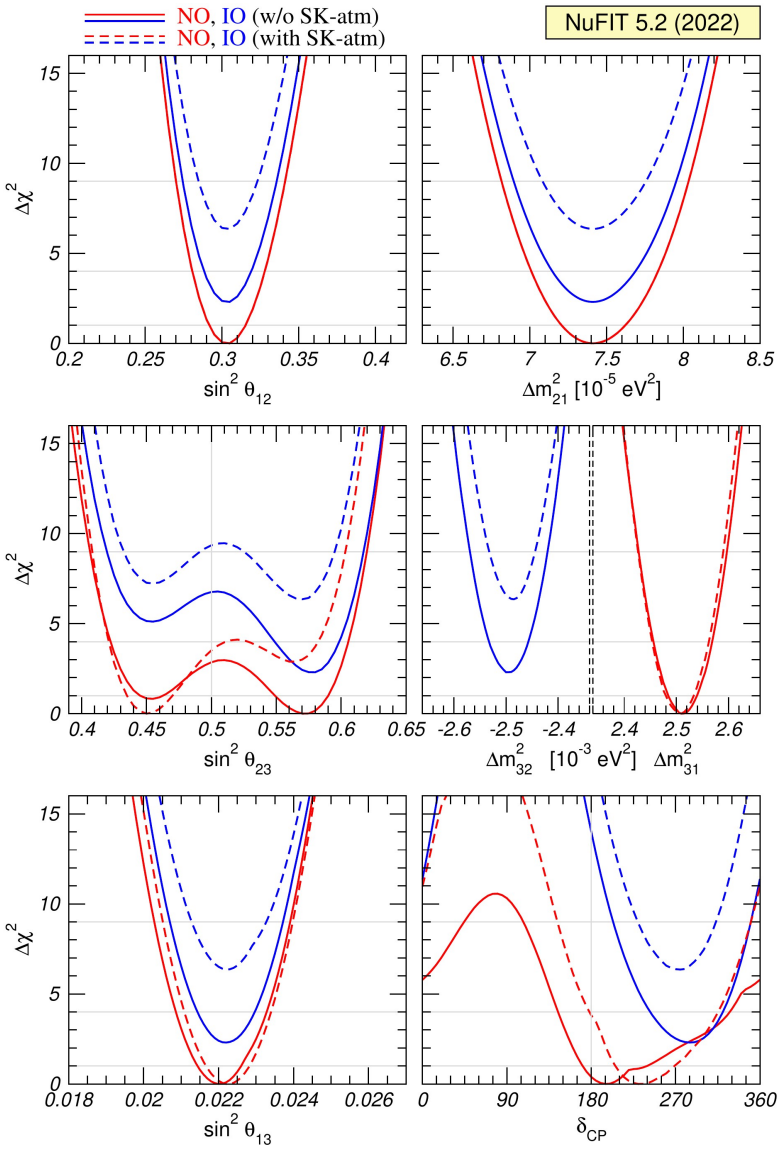

Figure 1.2: Global analysis of neutrino oscillation data. The red (blue) curves are for Normal (Inverted) Ordering [33].

The latest results from the global fit of neutrino experimental data as presented in NuFit 5.2 (2022) [33] are shown in Figure 1.2.

1.5 Massive Neutrinos

As mentioned earlier, the Standard Model of particle physics predicts that neutrinos have no mass. But, through various experiments on neutrino oscillation, it

has been proven that they do have mass. Therefore, one of the challenges that neutrino physics faces is the origin of neutrino mass. Another unknown property of neutrinos is whether they are of Dirac or Majorana nature. The nature of neutrinos are closely related to their mass generation. In the following section, we discuss the different mass terms- Dirac and Majorana mass terms.

1.5.1 Dirac Mass Term

The Dirac equation is given as

$$(i\gamma_\mu \partial^\mu - m)\Psi = 0, \tag{1.35}$$

The Dirac equation can be decomposed as follows

$$\begin{aligned} i\gamma_\mu \partial^\mu \Psi_L - m_D \Psi_R = 0 \\ i\gamma_\mu \partial^\mu \Psi_R - m_D \Psi_L = 0 \end{aligned} \tag{1.36}$$

These follow from the Lagrangian

$$\mathcal{L} = \mathcal{L}_{KE} + \mathcal{L}_D, \tag{1.37}$$

where

$$\begin{aligned} \mathcal{L}_{KE} &= i\bar{\Psi}\gamma_\mu \partial^\mu \Psi \\ &= i\bar{\Psi}_L \gamma_\mu \partial^\mu \Psi_L + i\bar{\Psi}_R \gamma_\mu \partial^\mu \Psi_R, \end{aligned} \tag{1.38}$$

and

$$\begin{aligned} \mathcal{L}_D &= -m_D \bar{\Psi}\Psi \\ &= -m_D \bar{\Psi}_R \Psi_L - m_D \bar{\Psi}_L \Psi_R, \end{aligned} \tag{1.39}$$

Note that the term in equation (1.38) treats the left and right-handed components independently. Also, the Dirac mass term connects the two components.

Let us express the Dirac neutrino in four component $\nu_D = \nu_L + N_R$, where ν_L and N_R denote the left and right-handed components, respectively. The mass terms of the Dirac neutrino arise from Yukawa interactions

$$-\mathcal{L}_{Dirac} = \bar{l}_L Y_\nu \tilde{\Phi} N_R + h.c., \tag{1.40}$$

After the SSB, we obtain

$$-\mathcal{L}'_{Dirac} = \bar{\nu}_L M_D N_R + h.c., \tag{1.41}$$

where $M_D = Y_\nu \langle \Phi \rangle$ with $\langle \Phi \rangle \simeq 174$ GeV is the *vev* of the Higgs field.

1.5.2 Majorana Mass Term

In neutrino physics, Majorana mass terms are a particular kind of mass term that considers neutrinos as their own antiparticles. To derive the Majorana mass term we start with a brief theory of Majorana fermions. Using the Majorana condition we can write,

$$\Psi = \Psi^C = \kappa C \bar{\Psi}^T, \tag{1.42}$$

where κ is an arbitrary factor. Applying this condition to the bi-spinors we get

$$\begin{pmatrix} \xi \\ \eta \end{pmatrix} = i \begin{pmatrix} 0 & \sigma_2 \\ -\sigma_2 & 0 \end{pmatrix} \begin{pmatrix} \xi^* \\ \eta^* \end{pmatrix} \tag{1.43}$$

Thus, Weyl spinor may be written as

$$\Psi = \begin{pmatrix} i\sigma_2 \eta^* \\ \eta \end{pmatrix}. \tag{1.44}$$

From equation (1.44), we can write a relation between the chiral components as

$$\begin{aligned} \Psi_L &= C \bar{\Psi}_R^T \\ \Psi_R &= C \bar{\Psi}_L^T. \end{aligned} \tag{1.45}$$

Using this convention Ψ may be written as

$$\Psi = \Psi_L + C \bar{\Psi}_L^T \tag{1.46}$$

and we get a corresponding mass term of the Majorana fermions as

$$\frac{1}{2} m (\bar{\Psi}_L^C \Psi_L + \bar{\Psi}_L \Psi_L^C) \tag{1.47}$$

Therefore, the Majorana mass term is given as

$$\begin{aligned} -\mathcal{L} &= \frac{m_M}{2}\left(\bar{\nu}_L \nu_L^C + h.c.\right) \\ &= \frac{m_M}{2}\left(\bar{\nu}_L C \bar{\nu}_L^T + h.c.\right) \\ &= \frac{m_M}{2}\bar{\nu}_M \nu_M \end{aligned} \tag{1.48}$$

The above mass term violates the lepton number by two units.

1.6 Seesaw Mechanism

An important component of effective field theory, which offers a theoretical foundation for understanding neutrino oscillations and tiny neutrino masses, is the Weinberg operator. After electroweak symmetry is broken and the Higgs field acquires a vacuum expectation value, the Weinberg operator in the Lagrangian plays a role in producing Majorana masses for the neutrinos. The Weinberg operator is given by [34]

$$\mathcal{O}_5 = \frac{\lambda}{\Lambda}\left(\bar{l}_L \tilde{\Phi}\right)\left(\Phi^\dagger \tilde{l}_R\right) \tag{1.49}$$

In this case, we omit writing flavor indices, λ represents a dimensionless coefficient, and Λ denotes the scale of New Physics. Three potential approaches exist for achieving ultraviolet (UV) completion of this operator at the tree level: type-I, type-II, and type-III seesaw mechanisms.

1.6.1 Type-I Seesaw

The Type I seesaw mechanism, an extension of the SM, offers a natural solution to the puzzle of why neutrino masses are exceedingly small. The seesaw mechanism, which adds heavy right-handed neutrinos to the Standard Model, was separately proposed by T. Yanagida [35] and by M. Gell-Mann, P. Ramond, and R. Slansky in the late 1970s. These right-handed neutrinos interact with the left-handed neutrinos and play a key role in the generation of neutrino masses. These right-handed neutrinos are singlet under the Standard Model gauge group and gauge

invariant Lagrangian may be written as

$$-\mathcal{L}_{mass} = \mathcal{L}_{Dirac} + \mathcal{L}_{Majorana} \tag{1.50}$$

where

$$\mathcal{L}_{Dirac} = -Y_D \bar{\nu} \Phi N_R + h.c., \tag{1.51}$$

with Y_D is the Dirac Yukawa coupling matrix and Majorana mass term for the right-handed neutrinos

$$\mathcal{L}_{Majorana} = -\frac{1}{2} M_R \bar{N}_R^c N_R + h.c., \tag{1.52}$$

with M_R being the Majorana mass matrix of N_R. The final Lagrangian of the mass term is

$$\mathcal{L}_{mass} = \frac{1}{2} \begin{pmatrix} \bar{\nu}_L^c & \bar{\nu}_R \end{pmatrix} \begin{pmatrix} 0 & m_D^T \\ m_D & M_R \end{pmatrix} \begin{pmatrix} \nu_L \\ \nu_R^c \end{pmatrix} + h.c. \tag{1.53}$$

With the assumption $m_D << M_R$, the diagonalization of the mass matrix by unitary transformation is given by

$$U^T \begin{pmatrix} 0 & m_D^T \\ m_D & M_R \end{pmatrix} U = \begin{pmatrix} M_{light} & 0 \\ 0 & M_{heavy} \end{pmatrix} \tag{1.54}$$

Thus, the eigenvalues give the mass of the light as well as the heavy neutrinos and are given by

$$M_{light} = m_\nu = M_D^T M_R^{-1} M_D, \tag{1.55}$$

Equation (1.55) is popularly known as the seesaw formula and

$$M_{heavy} = M_R \tag{1.56}$$

If we assume that Y_D is approximately of order 1 and that the scale of m_ν is around 0.05 eV, then it follows that the scale of M_R is approximately 10^{13} GeV, which is about the Grand Unified Theory scale.

1.6.2 Type-II Seesaw

Another extension of the Standard Model of particle physics is the Type-II seesaw which can account for the smallness of neutrino masses. Unlike the Type-I seesaw mechanism, which introduces heavy RH neutrinos, the Type II seesaw requires the inclusion of additional Higgs bosons with nontrivial lepton number [36–41]. Here, the SM is extended by adding an $SU(2)_L$ triplet Higgs scalar

$$\Delta = \begin{pmatrix} \frac{\Delta^+}{\sqrt{2}} & \Delta^{++} \\ \Delta^0 & -\frac{\Delta^+}{\sqrt{2}} \end{pmatrix}. \tag{1.57}$$

The Lagrangian contains a Dirac mass term that connects left-handed neutrinos to right-handed neutrinos via the Higgs doublet and the new Higgs triplet allows for a Yukawa interaction with the left-handed neutrinos.

$$-\mathcal{L}_{mass} = Y_D \bar{\nu}_L \Phi \nu_R + Y_T \bar{\nu}_L \tilde{\Delta} \nu_L + h.c., \tag{1.58}$$

where Y_T is the Yukawa coupling matrix and $\tilde{\Delta}$ is the conjugate of Δ. After EWSB, the neutrino mass matrix is given by

$$m_\nu = Y_\Delta v^2 \frac{\mu_\Delta}{M_\Delta^2}. \tag{1.59}$$

Due to the Type II seesaw, tiny neutrino masses are produced by creating a hierarchy between the electroweak scale and the scale linked to the Higgs triplet's *vev*. The Higgs triplet can produce unique collider signals that may be observable in experiments. Type II seesaw models may exhibit lepton flavor-violating processes that could be probed experimentally.

1.6.3 Type-III Seesaw

Another extension of the Standard Model of particle physics intended to address the smallness of neutrino masses is the Type III seesaw mechanism. The Type III seesaw provides new gauge interactions and the addition of fermionic triplet fields [42–45]. The additional fermionic $SU(2)$ triplet is represented by

$$\Sigma = \begin{pmatrix} \frac{\Sigma}{\sqrt{2}} & \Sigma^+ \\ \Sigma^- & -\frac{\Sigma}{\sqrt{2}} \end{pmatrix}. \tag{1.60}$$

For the triplet fermion the interaction Lagrangian is given by

$$-\mathcal{L}_\Sigma = \sqrt{2} Y_\Sigma \bar{L} \Sigma \tilde{\Phi} + \frac{1}{2} M_\Sigma \mathrm{Tr}\left(\bar{\Sigma}^c \Sigma\right) + h.c., \tag{1.61}$$

The mass eigenvalue of the light neutrino is given by

$$m_\nu \sim \frac{Y_\Sigma Y_\Sigma^T}{m_\Sigma}. \tag{1.62}$$

1.7 Baryon Asymmetry of the Universe

Another puzzle in particle physics and cosmology is the observed matter-antimatter imbalance of the universe. In this section, we first address several experimental results that support the presence of baryon number asymmetry. We then proceed to outline interesting dynamical scenarios intended to account for this asymmetry. Among various possible baryogenesis mechanisms, the leptogenesis mechanism stands out as especially intriguing because of its inherent relationship to the well-established seesaw mechanisms that explain the production of neutrino mass. As such, we focus on the details of the leptogenesis mechanism and present a thorough summary of its latest developments.

1.7.1 Evidence of Matter-Antimatter Asymmetry

It is a well-known fact in physics that there is nearly perfect symmetry in the fundamental interactions. The CPT theorem further articulates this symmetry, claiming that a particle and its antiparticle must have equal mass (and, if relevant, the same lifetime). This naturally gives rise to the notion that the larger universe ought to have the same symmetry between matter and antimatter as suggested by Dirac. Nevertheless, it is still unclear how the microscopic-scale Universe with equal proportions of matter and antimatter would lead to a symmetric macroscopic-scale Universe. Although the laws regulating individual particles point to a symmetry, the simple realization of a matter-antimatter symmetry is complicated and ambiguous when this symmetry is extrapolated to the cosmic scale [46].

There are two types of searches for antimatter: direct searches and indirect searches. As we do not observe any interactions that suggest that annihilation occurred between proton and anti-proton, it is evident that antimatter does not exist on Earth. High-energy accelerators, which create new particles and reactions through pp^- or e^+e^- collisions, store the most antimatter. The fact that humans have successfully conducted space travel proves that matter, not antimatter, makes up the solar system. The observation of cosmic rays provides further strong proof. If our galaxy or other galaxies possessed a substantial region of antimatter, we should have detected anti-matter in cosmic ray experiments.The observed anti-proton is supported by the outcomes of the reaction $p + p \rightarrow \bar{p} + 3p$ observed in cosmic rays.

Antimatter does not exist in the entire observable Universe, according to indirect searches. Matter-antimatter annihilations are likely to occur near the boundaries if there are substantial areas of antimatter. Diffuse gamma rays are the most valuable element for exploring matter-antimatter annihilation. Thorough examination indicates that the matter domain should span $d_0 = 10^3$ Mpc, which is simply the size of the visible Universe [47]. The analysis's approach is to suppose that the universe has a total baryon number of zero and that it is composed of matter and antimatter domains, each having a typical dimension of d_0. Subsequently, it is possible to compute the effects originating from the annihilation during the recombination period with existing observational data. The results are displayed in Figure 1.3 where it is clear that the situation with $d_0 = 10^3$ Mpc fits the data better, suggesting that there are no significant areas of antimatter in the observable Universe and that only matter is present.

1.7.2 Measurements from CMB and BBN

The baryon number density, denoted as η_B, plays a pivotal role in computing both the anisotropies of the Cosmic Microwave Background (CMB) and the initial abundances of light elements during Big Bang nucleosynthesis (BBN). From the

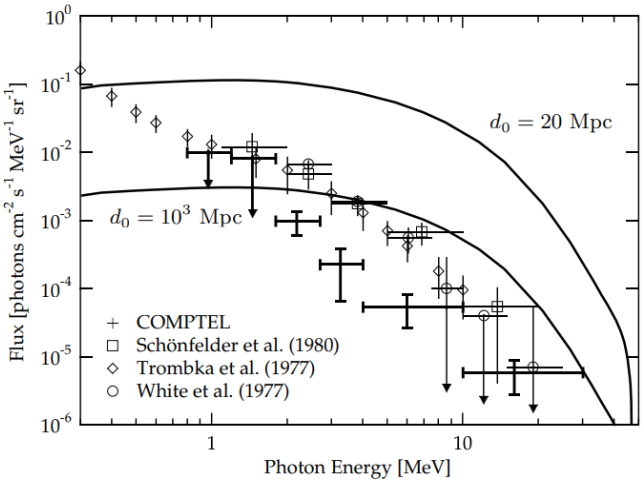

Figure 1.3: Comparing the estimated diffusive gamma-ray spectra from the matter-antimatter annihilation [47] with the observed one [48], where $d_0 = 20$ Mpc (upper solid curve) and $d_0 = 103$ Mpc.

five-year WMAP measurements as detailed in [49].

$$\eta_B = \frac{n_B - n_{\bar{B}}}{n_\gamma} = (6.21 \pm 0.16) \times 10^{-10}. \tag{1.63}$$

The outcome is obtained by measuring the primordial abundances of light elements, relying on the Big Bang Nucleosynthesis (BBN) theory. and the results found in Equation (1.63) are in good agreement with each other. As seen in Figure 1.4, the observed D and ^{7}Li number fractions, along with the measured ^{4}He mass fraction, may be used to calculate the cosmic baryon-to-photon ratio η_B. At the 95% confidence level, there is excellent consistency between the BBN concordance range of η_B and the CMB measurement of η_B. Interestingly, the results obtained from these two epochs- BBN ($t \gtrsim 1$s) and CMB ($t \sim 3.8 \times 10^5$ yr) are in agreement with each other. The dynamical origin of the universe's baryon number asymmetry, or baryogenesis, is a significant but unresolved issue in particle physics and cosmology.

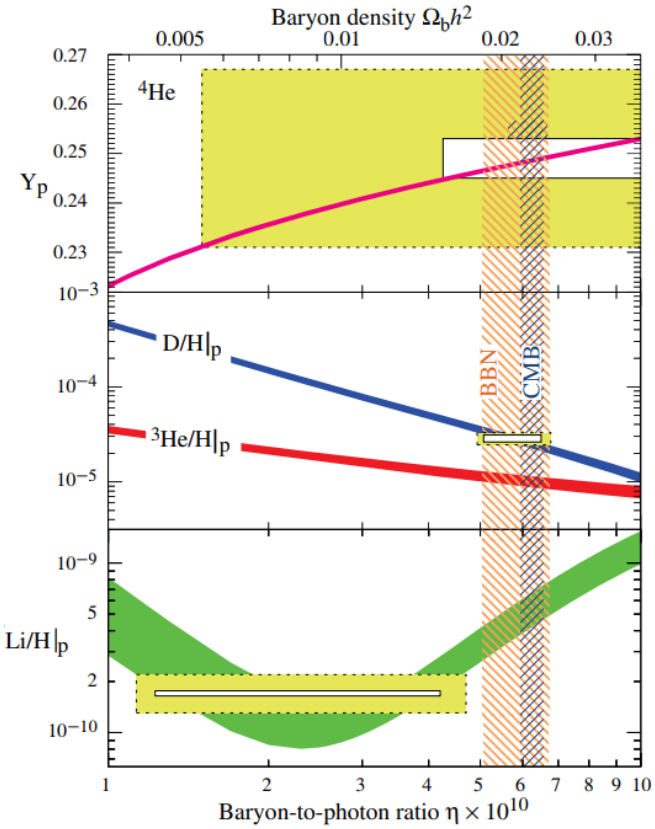

Figure 1.4: ^{4}He, D, and ^{7}Li primordial abundances predicted by the Big Bang Nucleosynthesis, where the bands show the ranges at the 95% confidence level [50]. CMB measurement of the cosmic baryon-to-photon ratio is represented by the vertical band.

1.7.3 Sakharov's Condition

In 1967, three prerequisites were put out by Soviet scientist Andrei Sakharov for the creation of baryon asymmetry in the early Universe. The set of requirements referred to as Sakharov's condition provides a structure for generating the observed imbalance between matter and antimatter, which leads to the dominance of baryonic matter in the universe. Below are the requirements set by Sakharov [51]:

1. Baryon number violation: If there is no baryon number B violation in the fundamental interactions, with $B = 0$ as a starting point, there would be

no gain in any baryon number as the Universe evolves. In the SM, at the classical level, baryon number (L) as well as lepton number (B) is conserved. However, considering the quantum level, it has been revealed that $B - L$ is precisely preserved in the Standard Model [52]. At the non-perturbative level, there exist interactions that violate the baryon number within the SM.

2. C and CP violation: CP violation suggests that there is a difference in the way the rules of physics regard particles and their antiparticles. To produce a net baryon asymmetry, there must be this distinction between matter and antimatter. In the Standard Model, CP violation is detected in the quark sector, specifically in the CKM matrix driving quark mixing. However, it is a known fact that the CP violation present in the CKM matrix cannot explain the origin of BAU.

3. Departure from Thermal Equilibrium: To create a net baryon asymmetry, departure from thermal equilibrium is necessary. There wouldn't be any net asymmetry if processes were in thermal equilibrium since matter and antimatter would be generated and destroyed in equal amounts.

1.7.4 Leptogenesis

Leptogenesis is a theoretical framework within the realm of particle physics and cosmology, providing explanations for the origin of the matter-antimatter asymmetry observed in the universe [53]. Leptogenesis is based on the asymmetrical decay of heavy right-handed neutrinos, which are added to the Standard Model to account for the seesaw process that explains the origin of tiny neutrino masses. A lepton asymmetry, mostly in the form of leptons (electrons and their neutrinos) over antileptons, is produced as these heavy neutrinos decay. This lepton imbalance is then converted into a baryon asymmetry by sphaleron processes, which are non-perturbative interactions in the electroweak sector that violate lepton and baryon numbers, leaving a residual net baryon excess in the Universe. The

flavour-dependent asymmetry produced from the decay of right-handed neutrino into lepton and Higgs is given by

$$\varepsilon_{i\alpha} = \frac{\Gamma\left(N_i \to l_\alpha + H\right) \; - \; \Gamma\left(N_i \to \bar{l}_\alpha + \bar{H}\right)}{\sum_\alpha \Gamma\left(N_i \to l_\alpha + H\right) \; + \; \Gamma\left(N_i \to \bar{l}_\alpha + \bar{H}\right)} \tag{1.64}$$

The scale of the masses of these RH neutrinos is model-dependent and may have different ranges in different models. In this thesis, we consider the case of low-scale leptogenesis $\sim \mathcal{O}(1)$ TeV. In the simplest scenario of thermal leptogenesis with a hierarchical mass spectrum of right-handed neutrinos, there is a lower bound on the mass of the lightest right-handed neutrino, $\mathrm{M}_1 \simeq 10^9$ GeV [54]. Although one can lower this limit if their masses are nearly degenerate, the scenario is popularly known as resonant leptogenesis [55, 56]. In such a situation, one-loop self-energy contribution is enhanced resonantly and the flavour-dependent asymmetry produced from the decay of right-handed neutrino into lepton and Higgs is given by [57–61]

$$\varepsilon_{i\alpha} = \sum_{i \neq j} \frac{\mathrm{Im}\left[\left(Y_\nu^*\right)_{\alpha i}\left(Y_\nu^*\right)_{\alpha j}\left(Y_\nu^\dagger Y_\nu\right)_{ij} + \xi_{ij}\left(Y_\nu^*\right)_{\alpha i}\left(Y_\nu^*\right)_{\alpha j}\left(Y_\nu^\dagger Y_\nu\right)_{ji}\right]}{\left(Y_\nu^\dagger Y_\nu\right)_{ii}\left(Y_\nu^\dagger Y_\nu\right)_{jj}} \cdot \frac{\xi_{ij}\zeta_j\left(\xi_{ij}^2 - 1\right)}{\left(\xi_{ij}\zeta_j\right)^2 + \left(\xi_{ij}^2 - 1\right)^2}. \tag{1.65}$$

where $\xi_{ij} = M_i/M_j$ and $\zeta_j = \left(Y_\nu^\dagger Y_\nu\right)_{jj}/(8\pi)$ with $Y_\nu = m_D/v$.

1.8 Outline of the Thesis

Chapter 2 provides a model in the minimal seesaw framework that uses the S_4 flavour symmetry group. Its main goal is to show how this model can produce trimaximal (TM_1) neutrino mixing patterns. Six parameters define the model, and the study incorporates global experimental data on neutrino oscillations. In addition, it explores the Majorana nature of neutrinos, mainly by examining neutrinoless double beta decay. The possibility of using the model to explain baryogenesis through resonant leptogenesis is also explored in this chapter. In the end, the results suggest that the model favours inverted hierarchy for neutrino masses.

Chapter 3 presents an explanation of the theoretical origin of neutrino mixing using the S_4 flavour symmetry. It is centred on an S_4 flavour symmetric model in the simplest inverse seesaw framework, which is intended to make sense of the data on neutrino oscillations that have been observed. The model has two gauge singlets and two extra right-handed neutrinos, extending the Standard Model. Additionally, the chapter delves into a gauge symmetry extension of the Standard Model with $S_4 \times Z_3 \times Z_4$ symmetry. A chi-squared analysis is included in the study to determine how well the model fits the experimental neutrino oscillation data. The chapter further explores the investigation of neutrinoless double beta decay within the model.

Chapter 4 focuses on the investigation of resonant leptogen- esis within the framework of a minimal radiative seesaw model. The minimum scotogenic model—which adds a Z_2 symmetry to the Standard Model gauge symmetry—is the subject of this work. This model investigates a situation with two almost degenerate right-handed neutrinos, which is essential for resonant leptogenesis and works especially well at lower temperatures. The neutrino mixing matrix's CP-violating phases are crucial in supplying the required CP violation for leptogenesis to occur successfully, which is necessary to account for the universe's observable baryon asymmetry (BAU). Neutrinoless double beta decay is investigated by analyzing the parameter space of the model, including limitations from successful baryogenesis.

Chapter 5 In the last study, we explore resonant leptogenesis in the minimal inverse seesaw (ISS) model, focusing on the ISS(2, 2) version. Together with two Standard Model gauge singlet neutrinos, this extension of the Standard Model adds two more right-handed (RH) neutrinos. We present a detailed investigation of the parameter space specific to the ISS(2, 2) model with the goal of determining leptogenesis-friendly settings. We consider cases in which low energy CP phases are the exclusive source of CP violation. Additionally, we study how the ISS(2, 2) model's parameter space for successful resonant leptogenesis is affected by a texture-zero configuration in the Dirac mass matrix.

Chapter 6 we summarize the main findings from their research and outline potential future directions for further exploration and advancement in this field of study.

Bibliography

[1] Fermi, E. An attempt of a theory of beta radiation. 1. *Z. phys* **88** (161), 19, 1934.

[2] Bethe, H. & Peierls, R. The "neutrino". *Nature* **133** (3362), 532–532, 1934.

[3] Reines, F. & Cowan Jr, C. Detection of the free neutrino. *Physical Review* **92** (3), 830, 1953.

[4] Goldhaber, M. *et al.* Helicity of neutrinos. *Physical Review* **109** (3), 1015, 1958.

[5] Davis Jr, R. *et al.* Search for neutrinos from the sun. *Physical Review Letters* **20** (21), 1205, 1968.

[6] Danby, G. *et al.* Observation of high-energy neutrino reactions and the existence of two kinds of neutrinos. *Physical Review Letters* **9** (1), 36, 1962.

[7] Fukuda, Y. *et al.* Evidence for oscillation of atmospheric neutrinos. *Physical Review Letters* **81**, 1562–1567, 1998.

[8] Ahmad, Q. R. *et al.* Measurement of the rate of $\nu_e + d \rightarrow p + p + e^-$ interactions produced by ^8B solar neutrinos at the sudbury neutrino observatory. *Phys. Rev. Lett.* **87**, 071301, 2001.

[9] Mikheyev, S. & Smirnov, A. Y. Resonant neutrino oscillations in matter. *Progress in Particle and Nuclear Physics* **23**, 41–136, 1989.

[10] Kuo, T.-K. & Pantaleone, J. Neutrino oscillations in matter. *Reviews of Modern Physics* **61** (4), 937, 1989.

[11] Kodama, K. *et al.* Detection and analysis of tau–neutrino interactions in donut emulsion target. *Nuclear Instruments and Methods in Physics Research Section A: Accelerators, Spectrometers, Detectors and Associated Equipment* **493** (1-2), 45–66, 2002.

[12] Group, P. D. *et al.* Review of particle physics. *Progress of Theoretical and Experimental Physics* **2020** (8), 083C01, 2020.

[13] Aker, M. *et al.* Improved upper limit on the neutrino mass from a direct kinematic method by KATRIN. *Physical review letters* **123** (22), 221802, 2019.

[14] Faessler, A. Status of the determination of the electron-neutrino mass. *Progress in Particle and Nuclear Physics* 103789, 2020.

[15] Obara, S. *et al.* Status of balloon production for KamLAND-Zen 800 kg phase. *Nuclear Instruments and Methods in Physics Research Section A: Accelerators, Spectrometers, Detectors and Associated Equipment* **845**, 410–413, 2017.

[16] Maki, Z. *et al.* Remarks on the unified model of elementary particles. *Progress of Theoretical Physics* **28** (5), 870–880, 1962.

[17] Tanabashi, M. *et al.* Review of particle physics: particle data groups. *Physical Review D* **98** (3), 1–1898, 2018.

[18] Cleveland, B. T. *et al.* Measurement of the solar electron neutrino flux with the homestake chlorine detector. *The Astrophysical Journal* **496** (1), 505, 1998.

[19] Hampel, W. *et al.* Final results of the 51cr neutrino source experiments in gallex. *Physics Letters B* **420** (1-2), 114–126, 1998.

[20] Altmann, M. *et al.* Complete results for five years of gno solar neutrino observations. *Physics Letters B* **616** (3-4), 174–190, 2005.

[21] Abdurashitov, J. *et al.* Measurement of the solar neutrino capture rate with gallium metal. iii. results for the 2002–2007 data-taking period. *Physical Review C* **80** (1), 015807, 2009.

[22] Achar, C. *et al.* Detection of muons produced by cosmic ray neutrinos deep underground. *Physics Letters B* **18** (2), 1965.

[23] Achar, C. *et al.* Observation of a non-elastic cosmic ray neutrino interaction. *Physics Letters B* **19** (1), 1965.

[24] Allison, W. *et al.* The atmospheric neutrino flavor ratio from a 3.9 fiducial kiloton-year exposure of soudan 2. *Physics Letters B* **449** (1–2), 137–144, 1999.

[25] Collaboration, K.-I. *et al.* Observation of a small atmospheric muon-neutrino/electron-neutrino ratio in kamiokande. *Phys. Lett. B* **280**, 146, 1992.

[26] Collaboration, T. *et al.* Indication of electron neutrino appearance from an accelerator-produced off-axis muon neutrino beam. *Physical Review Letters* **107** (4), 2011.

[27] Evans, J. *et al.* The minos experiment: results and prospects. *Advances in High Energy Physics* **2013**, 2013.

[28] Acero, M. *et al.* New constraints on oscillation parameters from ν e appearance and ν μ disappearance in the nova experiment. *Physical Review D* **98** (3), 032012, 2018.

[29] Bemporad, C. *et al.* Results from chooz. *Nuclear physics. B, Proceedings, supplements* **77** (1-3), 159–165, 1999.

[30] Abe, Y. *et al.* First measurement of θ_{13} from delayed neutron capture on hydrogen in the double chooz experiment. *Physics Letters B* **723** (1-3), 66–70, 2013.

[31] An, F. *et al.* Observation of electron-antineutrino disappearance at Daya Bay. *Physical Review Letters* **108** (17), 171803, 2012.

[32] Ahn, J. K. *et al.* Observation of reactor electron antineutrinos disappearance in the RENO experiment. *Physical Review Letters* **108** (19), 191802, 2012.

[33] Esteban, I. *et al.* The fate of hints: updated global analysis of three-flavor neutrino oscillations. *Journal of High Energy Physics* **2020** (9), 2020. URL `http://dx.doi.org/10.1007/JHEP09(2020)178`.

[34] Weinberg, S. Cosmological production of baryons. *Physical Review Letters* **42** (13), 850, 1979.

[35] Yanagida, T. Horizontal symmetry and masses of neutrinos. *Progress of Theoretical Physics* **64** (3), 1103–1105, 1980.

[36] Gu, P.-H. *et al.* Neutrino masses, leptogenesis, and dark matter in a hybrid seesaw model. *Physical Review D* **79** (3), 2009.

[37] Gu, P.-H. *et al.* Double type-ii seesaw scenario, baryon asymmetry, and dark matter for cosmic $e^{\pm}$ excesses. *Physical Review D* **80** (5), 2009.

[38] Sierra, D. A. *et al.* Scalar triplet flavored leptogenesis: a systematic approach. *Journal of Cosmology and Astroparticle Physics* **2014** (08), 003–003, 2014.

[39] Chao, W. *et al.* Neutrino mixing and leptogenesis in type-ii seesaw scenarios with left–right symmetry. *Physics Letters B* **659** (1–2), 281–289, 2008.

[40] McDonald, J. *et al.* Type-ii seesaws at colliders, lepton asymmetry and singlet scalar dark matter. *Journal of Cosmology and Astroparticle Physics* **2008** (04), 037, 2008.

[41] Antusch, S. & King, S. F. Leptogenesis in unified theories with type ii see-saw. *Journal of High Energy Physics* **2006** (01), 117–117, 2006.

[42] Brahmachari, B. *et al.* Supersymmetric model of neutrino mass and leptogenesis with string-scale unification. *Physics Letters B* **520** (1–2), 152–158, 2001.

[43] Hambye, T. *et al.* Constraints on neutrino masses from leptogenesis models. *Nuclear Physics B* **695** (1–2), 169–191, 2004.

[44] Blanchet, S. & Fileviez Pérez, P. Baryogenesis via leptogenesis in adjoint SU(5). *Journal of Cosmology and Astroparticle Physics* **2008** (08), 037, 2008.

[45] Aristizabal Sierra, D. *et al.* Implications of flavor dynamics for fermion triplet leptogenesis. *Journal of High Energy Physics* **2010** (10), 2010.

[46] Steigman, G. Observational tests of antimatter cosmologies. *Annual Review of Astronomy and Astrophysics* **14** (1), 339–372, 1976.

[47] Cohen, A. G. *et al.* A matter-antimatter universe? *The Astrophysical Journal* **495** (2), 539, 1998.

[48] Kappadath, S. *et al.* The preliminary cosmic diffuse gamma-ray spectrum from 800 kev to 30 mev measured with comptel. In *24th International Cosmic Ray Conference, Vol. 2, held August 28-September 8, 1995 in Rome, Italy. Edited by N. Iucci and E. Lamanna. International Union of Pure and Applied Physics, 1995., p. 230*, vol. 2. 230, 1995.

[49] Komatsu, E. *et al.* Measuring primordial non-gaussianity in the cosmic microwave background. *The Astrophysical Journal* **634** (1), 14, 2005.

[50] Cyburt, R. H. *et al.* Big bang nucleosynthesis: Present status. *Reviews of Modern Physics* **88** (1), 2016.

[51] Sakharov, A. D. The initial stage of an expanding universe and the appearance of a nonuniform distribution of matter. *Sov. Phys. JETP* **22**, 241, 1966.

[52] t Hooft, G. Symmetry breaking through bell-jackiw anomalies. *Physical Review Letters* **37** (1), 8–11, 1976.

[53] Fukugita, M. & Yanagida, T. Barygenesis without grand unification. *Physics Letters B* **174** (1), 45–47, 1986.

[54] Davidson, S. & Ibarra, A. A lower bound on the right-handed neutrino mass from leptogenesis. *Physics Letters B* **535** (1-4), 25–32, 2002.

[55] Pilaftsis, A. & Underwood, T. E. Resonant leptogenesis. *Nuclear Physics B* **692** (3), 303–345, 2004.

[56] Pilaftsis, A. CP violation and baryogenesis due to heavy majorana neutrinos. *Physical Review D* **56** (9), 5431, 1997.

[57] Xing, Z.-z. & Zhang, D. Bridging resonant leptogenesis and low-energy CP violation with an RGE-modified seesaw relation. *Physics Letters B* **804**, 135397, 2020.

[58] Pilaftsis, A. Resonant CP violation induced by particle mixing in transition amplitudes. *Nuclear Physics B* **504** (1-2), 61–107, 1997.

[59] Anisimov, A. *et al.* The CP-asymmetry in resonant leptogenesis. *Nuclear Physics B* **737** (1-2), 176–189, 2006.

[60] De Simone, A. & Riotto, A. On resonant leptogenesis. *Journal of Cosmology and Astroparticle Physics* **2007** (08), 013, 2007.

[61] Francis, N. K. & Singh, N. N. Validity of quasi-degenerate neutrino mass models and their predictions on baryogenesis. *Nuclear Physics B* **863** (1), 19–32, 2012.